6450 nm wavelength tissue ablation using a nanosecond laser based on difference frequency mixing and stimulated Raman scattering

G. S. Edwards,[1,*] R. D. Pearlstein,[1] M. L. Copeland,[2] M. S. Hutson,[3] K. Latone,[4] A. Spiro,[4] and G. Pasmanik[4]

[1]*Free-Electron Laser Laboratory, Duke University, Durham, North Carolina 27708, USA*
[2]*Northern Rockies Neurosurgeons, Billings, Montana 59101, USA*
[3]*Department of Physics and Astronomy, Vanderbilt University, Nashville, Tennessee 37235, USA*
[4]*Passat, Inc., Linthicum, Maryland 21090, USA*
[*]*Corresponding author: edwards@fel.duke.edu*

Received January 26, 2007; revised March 2, 2007; accepted March 9, 2007;
posted March 19, 2007 (Doc. ID 79462); published April 30, 2007

A four-stage laser system was developed, emitting at a wavelength of 6450 nm with a 3–5 ns pulse duration, ≤2 mJ pulse energy, and 1/2 Hz pulse repetition rate. The laser system successfully ablated rat brain tissue, where both the collateral damage and the ablation rate compare favorably with that previously observed with a Mark-III Free-Electron Laser.

OCIS codes: 140.3070, 170.1020, 170.3890.

While lasers are in routine use for a range of medical protocols, there has not been broad acceptance of a neurosurgical laser. The Mark-III Free-Electron Laser (FEL), when operating near 6450 nm, efficiently ablates soft tissue with minimal collateral thermal damage and has been used successfully in human brain and animal ophthalmic surgeries [1]. This FEL is based on accelerator technology, a major factor driving up its size and cost and thus limiting its acceptance. Consequently, there has been interest in the development of a relatively compact and less expensive ~6450 nm laser for human surgical applications. A gas discharge strontium vapor laser has been investigated, but it produced unacceptable collateral thermal damage [2].

When exploring alternative laser technologies for soft tissue ablation, it is important to consider the role of the FEL superpulse structure, which includes 4–6 μs bursts of picosecond pulses at a repetition rate of 2.85 GHz [1]. Previous investigations suggested the preferential FEL ablation properties are due to the high average power during the 4–6 μs bursts and not the picosecond pulses *per se* [1,3]. Theoretical modeling indicated that the key dynamics occur on the 10 ns time scale, subject to constraints in energy and power densities [4], motivating our interest in the development of a nanosecond pulsed 6450 nm laser.

Here we report the development of a 6450 nm nanosecond laser that ablates brain tissue with acceptable collateral thermal damage. The design strategy is based on difference frequency mixing (DFM) and stimulated Raman scattering (SRS) [Fig. 1(a)]. Stages 1 through 3 are based on a recent advancement in DFM of the frequency-doubled emission of a solid-state laser with the Raman-shifted emission from the same laser [5]. DFM provides effective conversion of the laser emission at frequency ω to the anti-Stokes Raman component at $\omega+\Omega_1$. Effective generation of the anti-Stokes components in DFM significantly expands the range of frequencies that can be used in stage 4, where Stokes conversion provides an output emission frequency $\omega_{out}=(\omega+\Omega_1)-n\Omega_2$, where n indicates the order of the Stokes component.

The implementation [Fig. 1(b)] produced nearly TEM_{00} emission of 6450 nm, 3–5 ns pulse duration, and pulse energies ≤2 mJ. A flash-lamp Nd:YLF master oscillator-power amplifier system was the source of 1053 nm radiation ($\lambda=2\pi c/\omega$) with a 12 ns pulse duration. High-quality rods for the Nd:YLF master oscillator were necessary to avoid degradation in performance (Northrop Grumman, Charlotte, North Carolina). The 1053 nm beam was first amplified (Amplifier 1) and then divided into two beams. One beam was Raman converted to 1095 nm by SRS in liquid $SnCl_4$ ($\Omega_1=368$ cm^{-1}). The other beam was amplified (Amplifier 2) and frequency doubled to 526.5 nm in a KDP crystal. Both beams were recombined for DFM using $RbTiOPO_4$ (RTP) crystals to produce 1014 nm light. The 1014 nm emission was then converted by SRS in a high-pressure H_2 cell into the second Stokes component ($\Omega_2=4155.5$ cm^{-1}, $n=2$), resulting in the output emission at 6450 nm.

One key issue for optimization involves the efficiency of the Raman liquid laser. There is a competition between SRS and stimulated Brillouin scattering (SBS) when operating with 10–15 ns pulses since the SRS threshold in most liquids is higher than the SBS threshold. To improve the efficiency of the SRS excitation in $SnCl_4$, an auxiliary phase conjugating mirror in Amplifier 1 shortened the laser pulse front of the 1053 nm emission to 2 ns and the full width at half-maximum (FWHM) to 4–6 ns. In addition, the SRS threshold was reduced by excitation of Stokes Raman emission in an optical resonator. Selective

0146-9592/07/111426-3/$15.00

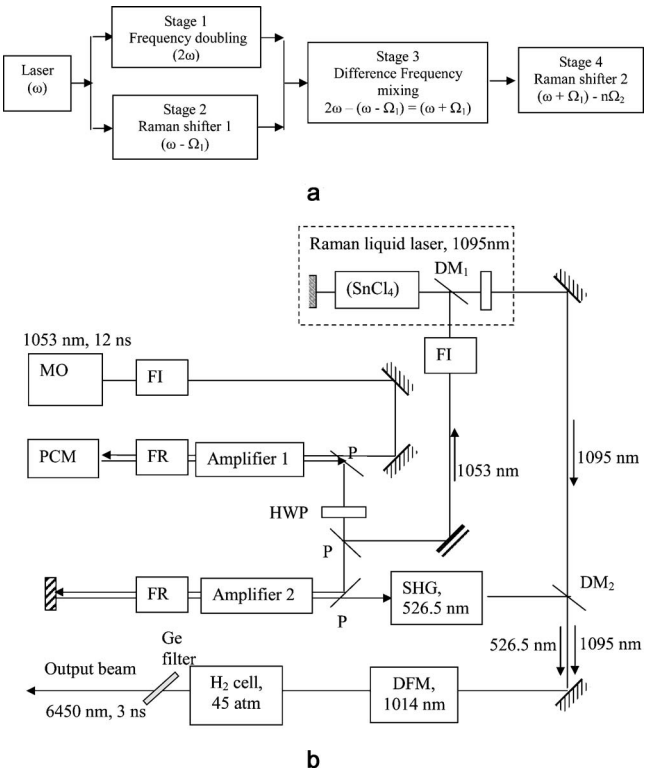

Fig. 1. a, Design strategy and b, optical diagram. MO is the passively *Q*-switched master oscillator (Nd:YLF rod ∅ 5 mm × 60 mm). Nd:YLF Amplifiers 1 (rod ∅ 6.3 mm × 105 mm) and 2 (rod ∅ 15 mm × 110 mm) are each two-pass. PCM, phase conjugating mirror; FI, Faraday isolator; FR, Faraday rotator; P, polarizer; HWP, half-wave plate; SHG, second-harmonic generator (KDP crystal); DM_1, DM_2, dichroic mirrors. DFM is two RTP crystals, each 6 mm × 20 mm × 25 mm.

mirror DM1 in the resonator reflected the 1053 nm pumping emission towards the $SnCl_4$ cell, passed the 1095 nm Raman component, and reflected the SBS emission from the Raman cell out of the resonator, thereby suppressing SBS amplification. The fast Raman process dominated SBS at the sharp front, making it possible to increase the SRS output from the resonator with practically no pulse compression. With 20 mJ pumping pulses, the Raman output at 1095 nm was 2–3 mJ and the pulse width at the FWHM was 3.5–4.0 ns.

A second key issue for optimization involves the difference frequency mixer. High DFM energy conversion efficiency is achievable with optimization of the 526.5 nm pumping power density and the RTP crystal length. Two RTP crystals were used for DFM, with an efficiency of ~15–20%. The crystals were designed for *oee* three-wave parametrical interaction: 526.5 nm(e) → 1014 nm(e) + 1095 nm(o). The maximum possible DFM efficiency of 25% for the 50 mm total crystal length is achievable when the power density of 526.5 nm emission is 20–30 MW/cm^2. A prism expander (not shown) before the RTP crystals stretched the incident beam in one direction, adjusting the power density to maximize the DFM output. The DFM output emissions at two wavelengths (1014 and 1095 nm) had orthogonal polarizations and approximately the same energy: E(1014 nm) ≈ E(1095 nm) ≈ 40 mJ ± 5 mJ. The DFM output pulse duration was 3.5–4.0 ns.

The final Raman converter was based on a cylindrical cell filled with pressurized H_2 (45 atm). To increase conversion efficiency, both the 1014 and 1095 nm emissions were focused in the cell. Additional 1095 nm pumping helped to excite a phonon grating, which produced Raman scattering of 1014 nm light. A germanium filter placed at the Brewster angle after the H_2 cell cut off all wavelengths below 2000 nm, i.e., pumping emission and the first Stokes components. Since the Raman gain at λ_{2S} of the 2nd Stokes is proportional to $\lambda_{2S}^{-3/2}$, excitation of the second Stokes component from 1095 nm emissions at 12,200 nm is not expected. Any residual emission at 12,200 nm is suppressed by the germanium filter due to orthogonal polarizations at 6450 and 12,200 nm.

We evaluated laser ablation of brain tissue (necropsy specimens, Sprague-Dawley rats) in two sets of experiments. For both sets, brains were prepared by perfusing *in situ* with 4% paraformaldehyde in 0.1 M phosphate buffered saline (PBS, pH 7.4), equilibrated at 4 °C in 30% sucrose, and then frozen in Optimal Cutting Temperature compound (Ted Pella Inc., Redding, California) at −80 °C until sectioning. Coronal sections from the mid-cerebrum were cut using a cryostat, then floated in ice cold PBS. Immediately before laser irradiation, tissue sections were transferred to a glass microscope slide, brought to room temperature, and blotted to remove excess buffer solution. The first set of experiments aimed to achieve full thickness ablation. Given the uncertainty associated with these initial experiments, we irradiated sections of 20 μm (N=4), 100 μm (N=1), 150 μm (N=1), and 200 μm (N=2) thickness with a large number of pulses (100 or 200) using a tightly focused beam (theoretical diameter of ~65 or ~125 μm). The energy per pulse was ~1 mJ, where each pulse satisfied the model prediction for soft tissue ablation [4], and two sites on each section were targeted [Fig. 2(a)]. The tissue was then placed in PBS at 4 °C. Brain tissue sections were initially examined using a 15–300× stereoscopic microscope (Leica) with surface illumination, then stained with hematoxylin–eosin to better characterize the borders of the full thickness ablation cavities.

For both the 20 and 100 μm sections, 100 pulses resulted in full thickness incisions for both spot sizes. For both 150 and 200 μm sections, irradiation with 200 pulses focused to a diameter of ~65 μm resulted in full thickness incisions. On the whole, the boundaries of ablation cavities were sharply demarcated. While we infrequently observed signs of coagulative changes, carbonization, or tissue fragmentation after staining, a zone of dense staining extending a maximum distance of 22 ± 5 μm (mean ± SD, N=5) into the tissue was observed indicating protein denaturation/tissue dehydration [Fig. 2(b)].

The second set of experiments aimed to achieve partial thickness incisions. For these studies, 200 μm

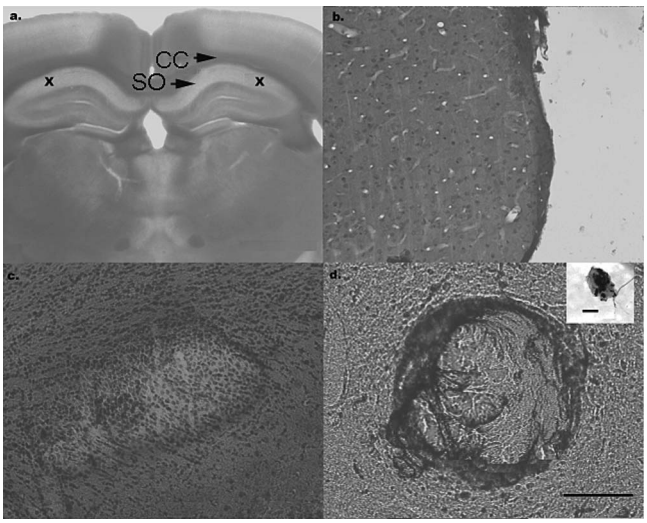

Fig. 2. Ablation in 200 μm thick tissue sections: a, Targets for laser irradiation (X) within the stratum oriens (SO); CC indicates corpus callosum. X–X distance is 6 mm. b, Side view of a full thickness ablation (200 pulses, 0.89 ± 0.08 mJ/pulse, $\sim$65 μm spot size). c, Stained section of a partial thickness ablation cavity (60 pulses, 0.83 ± 0.02 mJ/pulse, $\sim$100 μm spot size). The ellipsoid shape is due to beam wander. d, Ablation cavity of an unstained section (60 pulses, 0.83 ± 0.02 mJ/pulse, $\sim$100 μm spot size), including a carbonized deposit (inset, 10 μm scale bar). For b–d, the scale bar is 100 μm.

thick sections received 60 pulses at each spot, where the theoretical diameter of the focused beam was $\sim$100 μm. Sections were examined prior to and after staining. Partial thickness incisions were observed in all stained sections. Cell morphology was typically normal along the walls and floor of the ablation cavity [Fig. 2(c)], i.e., the perimeter of the cavity indicated the presence of the laser incision. There was no evidence of damage to the neighboring white matter tracts or CA1 pyramidal cells. Carbonized deposits and evidence of coagulated tissue were occasionally, but not consistently, observed within the ablation cavity in the unstained sections [Fig. 2(d)]. In contrast to the coagulative changes traditionally found in collateral thermal injury, the collateral damage reported here compares favorably with FEL brain surgery where the cells immediately adjacent to surface cells had well-defined nuclear morphology [1].

To approximate the ablation rate, Z-stack images of partial thickness laser incisions were collected at 500 nm intervals using an Olympus BX61 microscope. Measured depth, scaled to correct for tissue shrinkage during dehydration, approximates the average ablation rate to be 0.64 ± 0.03 μm/mJ at a spot size of $\sim$100 μm diameter ($N=3$). This is less than half the average value observed previously in FEL brain tissue ablation [1], where there was no correction for tissue shrinkage. This difference may also be attributable to using fixed tissue, which was not the case in the previous study. Unfixed tissue is subject to enzymatic digestion; tissue fixation inactivates these enzymes by cross-linking proteins. Both processes affect the physical properties of brain tissue, but in opposite directions. In addition, the theoretical model predicts that one consequence of a nanosecond pulse train relative to the FEL superpulse is a reduction in the amount of protein denaturation by $\sim$10% [4], which may also contribute to this difference. Based on previous clinical experience with the FEL [1], we project that the average optical power will need to increase by about two orders of magnitude to achieve sufficient ablation rates for human surgery, where the current laser system delivered about a milliwatt of optical power.

In conclusion, the nanosecond laser system described here can ablate brain tissue with acceptable collateral thermal damage. These findings suggest that surgical ablation of the central nervous system can be controlled at the level of a single cell thickness. While these tissue ablation studies confirm the model prediction with regard to collateral thermal damage, in the future it will be necessary to increase the optical power to achieve an acceptable ablation rate. Since scaling the pulse energy is limited by optical breakdown in H_2, increasing the pulse repetition rate is the most promising strategy.

We acknowledge support from the NIH (R43 RR018435) and the Department of Defense Medical Free Electron Laser Program (N00014-99-1-0891 and F49620-00-1-0370).

References

1. G. S. Edwards, R. H. Austin, F. E. Carroll, M. L. Copeland, M. E. Couprie, W. E. Gabella, R. F. Haglund, B. A. Hooper, M. S. Hutson, E. D. Jansen, K. M. Joos, D. P. Kiehart, I. Lindau, J. Miao, H. S. Pratisto, J. H. Shen, Y. Tokutake, L. van der Meer, and A. Xie, Rev. Sci. Instrum. **74**, 3207 (2003), and references therein.
2. M. A. Mackanos, B. Ivanov, A. N. Soldatov, I. Kostadinov, M. H. Mendenhall, D. W. Piston, R. F. Haglund, and E. D. Jansen, Proc. SPIE **5319**, 201 (2004).
3. M. A. Mackanos, J. A. Kozub, and E. D. Jansen, Phys. Med. Biol. **50**, 1871 (2005).
4. M. S. Hutson, S. A. Hauger, and G. Edwards, Phys. Rev. E **65**, 061906 (2002).
5. S. Kuznetsov, G. Pasmanik, A. Shilov, and L. Tiour, Opt. Lett. **29**, 848 (2004).